applied sciences

MDPI

Article

Study on the Selection of Coil Energization Directions in Multistage Synchronous Induction Coil Launcher

Jiayu Kang, Yuan Guan and Xiaobo Wan *

The School of Electrical and Control Engineering, Shaanxi University of Science and Technology, Xi'an 710021, China; kangjiayu@sust.edu.cn (J.K.); 19927450313@163.com (Y.G.)
* Correspondence: wxb2099@163.com

Abstract: In order to enhance the initial velocity and energy conversion efficiency of multi-stage synchronous induction coil launchers, the direction of coil energization for the drive coils is studied. There are typically two energization methods for multi-stage launching devices: (1) PP (Positive-Positive), where positive current is applied to all drive coils, and (2) PN (Positive-Negative), where currents in opposite directions are alternately applied to the drive coils. A finite element model of a four-stage coil launcher is established in ANSYS2022R2, and the acceleration effects of the armature under different inter-stage distances are analyzed for two energization methods. The study reveals that the PN configuration does not always result in higher armature velocities compared to the PP configuration under different inter-stage distances. The theoretical explanation is provided for the variations in the forces exerted by the previous and next drive coils on the armature during the acceleration process. It is found that the magnitude of the induced current in the previous and next drive coils during the launch process is influenced by the inter-stage distance, which in turn affects the electromagnetic thrust coupled with the armature. Thus, the method of determining the direction of current in the launching device coil is obtained.

Keywords: electromagnetic launcher (EML); energization method; finite elements model; inter-stage distance; synchronous induction coil launcher (SICL)

Citation: Kang, J.; Guan, Y.; Wan, X. Study on the Selection of Coil Energization Directions in Multistage Synchronous Induction Coil Launcher. *Appl. Sci.* **2024**, *14*, 5663. https://doi.org/10.3390/app14135663

Academic Editor: Alessandro Lo Schiavo

Received: 20 May 2024
Revised: 21 June 2024
Accepted: 27 June 2024
Published: 28 June 2024

1. Introduction

Electromagnetic launching technology can solve many bottleneck problems encountered in the development of traditional artillery. It is a critical area of focus for the advancement of future military technology and is increasingly becoming a leading research field in various countries [1]. The synchronous induction coil launcher, when operating in multiple stages, functions similarly to a linear synchronous motor. The current on its armature is induced by the synchronous pulse discharge of the multi-stage drive coils [2]. Researchers have primarily enhanced the launching performance of the device by adjusting the parameters of the launching device, driving power supply, and trigger parameters [3–5]. In recent years, it has been discovered that the magnetic field distribution produced by introducing reverse current into one or multiple drive coils improves the final exit velocity and energy conversion efficiency. As a result, researchers have initiated studies on introducing different current directions into the drive coils, both domestically and internationally.

Earlier, the Sandia National Laboratories in the United States discovered that changing the arrangement of the adjacent drive coils' polarity in the multi-stage SICL could enhance the launching performance. Ingram et al. initially proposed two different energization methods to address this phenomenon [6]. These methods involve passing current in the same direction or alternating reverse direction in the drive coils, referred to as the PP launcher and PN launcher, respectively. They concluded that the PN launcher, by

adjusting the armature trigger position, would provide a higher armature velocity. Similarly, Zhang Tao et al. suggested that it is feasible to change the magnetic field direction to improve the system's launching performance, which was verified by a 15-stage coil gun [7]. From the perspective of the armature acceleration mechanism, they analyzed the armature movement law and current distribution under two magnetic field directions and proposed that the armature acceleration mainly occurs during the falling edge of the drive coil current [8–10]. Niu Xiaobo et al. improved the energy conversion efficiency by delaying the polarity reversal of the coil to reduce the larger braking force caused by the polarity reversal process [11]. Ram Ranashree's team analyzed and explained the reasons why the optimal armature position in each stage coil of the PP and PN configurations is different and why the PN launcher achieves a higher launching velocity [12].

Some researchers have observed that using the PN configuration energization method can enhance the launch performance of the coil device. However, there is currently no explanation within the known scope regarding when to choose the PN configuration and whether it is suitable for all devices [13]. Building upon previous research, this article conducts an in-depth study on the PN configuration of the SICL, which alternately introduces currents of different directions into each stage drive coil. Through finite element simulation analysis, the launch performance differences between the PP and PN energization methods are compared. It is worth noting that during the simulation optimization process of different parameter devices, it is discovered that introducing reverse current into the drive coils alternately can have varying effects on the acceleration performance of the adjusted device. This means that after optimization adjustments, the phenomenon of the PP configuration being superior to the PN configuration arises, and not all devices will achieve better performance under the optimized PN configuration.

Researchers have previously focused on the study of PN configuration launch devices based solely on the results obtained from their own device parameters. While researchers like Ram Ranashree and Zhang Tao et al. have found that the PN configuration is more favorable for the launcher performance of the device, their results are only applicable to their own device parameters, lacking generalizability. This study delves into the launch effects of the PN configuration, revealing that the distance between drive coils affects the acceleration effects of the two configurations. By fundamentally analyzing the acceleration characteristics of the two configurations, more universal conclusions are drawn, providing a certain basis for the selection of the coil energization direction.

By adjusting the distance between each stage drive coil (inter-stage distance), two completely opposite simulation results can be obtained. That is, after optimizing and adjusting the launching device, two simulation outcomes emerge: the armature velocity is better in the PP configuration compared to the PN configuration, and the PN configuration armature velocity is better than the PP configuration. Therefore, this article focuses on a four-stage SICL as an example to investigate how the inter-stage distance affects the armature velocity in these two configurations. The inherent relationship between the inter-stage distance and the choice of energization method for the launching device is analyzed and confirmed through simulation. This connection can be used as the basis for determining the energization direction of the device.

2. Simulation Model Establishment

2.1. Finite Element Analysis

This article utilizes the transient analysis module of Maxwell v.2022R2 software to conduct simulation calculations on the SICL device. By coupling the circuit-field method and finite element analysis method, the electromagnetic field equations of the coil in the vertical launching device are coupled with external control circuit equations for solving, reflecting the transient motion process of the launching system.

In the transient solver module, the $T-\Omega$ method is employed for solving [5,7], describing electromagnetic transients through the following three Maxwell equations.

$$\begin{cases} \nabla \times H = \sigma E \\ \nabla \times E = -\dfrac{\partial B}{\partial t} \\ \nabla \cdot B = 0 \end{cases} \tag{1}$$

where E is the induced electric field intensity; B is the magnetic flux density; H is the magnetic field intensity; σ is the material's electrical conductivity; and t is time.

Choose function S to satisfy

$$S = -\int \phi dt \tag{2}$$

Furthermore, let

$$A' = A - \nabla S = A + \int \nabla \phi dt \tag{3}$$

$$\phi' = \phi + \frac{\partial S}{\partial t} = 0 \tag{4}$$

In the Coulomb gauge $\nabla \times A' = 0$, the governing equations for the electromagnetic field are expressed as:

$$\begin{cases} \sigma \dfrac{\partial (A + \nabla \phi)}{\partial t} + \nabla \times (\mu \nabla \times A) = J_s \\ \nabla \left[\sigma \dfrac{\partial (A + \nabla \phi)}{\partial t} - J_s \right] = 0 \end{cases} \tag{5}$$

In Equation (5), ϕ represents scalar electric potential; A signifies vector magnetic potential; J_s represents current density; and μ is the magnetic permeability. If we neglect the eddy current in the driving coil conductor region, the relationship between total conductor current and current density J_s is as follows:

$$J_s = \frac{N_c}{S_c} i(t) \tag{6}$$

In Equation (6), S_c represents the cross-sectional area of the winding and N_c stands for the number of turns in the coil.

The electromagnetic field control equation obtained from the finite element analysis serves as the foundation for software solutions. By utilizing Maxwell software, it is possible to obtain curves depicting the variation of various parameters over time during the launching process, as well as the distribution patterns of the electromagnetic field.

2.2. Finite Element Model of SICL

In this article, a finite element model of a four-stage SICL is established. In the external circuit simulation model, a pulse power supply system model is established, and ANSYS Maxwell is used for coupled field-circuit simulation analysis [14]. Taking advantage of the strengths of both the field model and the circuit model, the transient launching process of the induction coil device is simulated [15,16].

During the process of electromagnetic coil launch, the armature is suspended and accelerated without contact with the launch pipeline. Therefore, it is assumed that the central axis of the armature coincides with the central axis of the launching tube during the whole launching process, that is, the axis of the armature does not deviate from the axis of the drive coil. Under this condition, the three-dimensional launching system model is simplified into a two-dimensional axisymmetric simulation model, which is modeled in cylindrical coordinates. The two-dimensional finite element simulation model of the

four-stage SICL established in Maxwell is shown in Figure 1. This diagram displays the key components of the drive coils and armature used in our ANSYS simulations, essential for understanding the impact of different energization methods analyzed in the study. The parameters of the simulation model for the launching device are shown in Table 1. This table lists essential specifications such as dimensions and materials for the drive coils and armature.

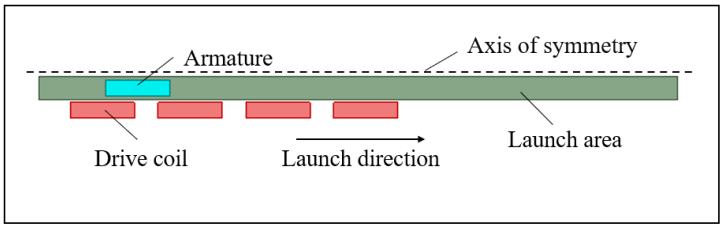

Figure 1. The simulation model of four-stage SICL.

Table 1. The simulation model parameters of the launching device.

Component	Parameter	Value
Drive coil (1–4 stages)	Inner radius (mm)	43
	Thickness (mm)	5
	Length (mm)	20
	Turns	40
	Material	Copper
Armature	Inner radius (mm)	36
	Thickness (mm)	5
	Length (mm)	20
	Mass (g)	50
	Material	Aluminum

Studying the parameter characteristics of the induction coil launch device is the basis for conducting research on coil launch devices. For a multi-stage induction coil launch device, as the driving coil accelerates the armature stage by stage, the speed at which the armature enters the driving coil increases. To improve the launch efficiency of the device, selecting appropriate device parameters involves analyzing the characteristics of each parameter as the armature entry speed increases. The two-dimensional schematic diagram of the coil launching device in this study is shown in Figure 2. The armature is launched in the direction of the arrow in the diagram, with a distance D = 5 mm between each stage of driving coils. The armature is progressively accelerated by four stages of coils. P_1 represents the triggering position of the armature in the first-stage driving coil, while T_i (where i = 2, 3, and 4) represents the triggering time of the armature in the second- to fourth-stage driving coils. The driving coils are powered at the appropriate triggering times to accelerate the armature forward. Not all structural and electrical parameters of multi-stage induction coil devices need to be optimized. In this study, the armature to be launched is predetermined, and the armature parameters cannot be adjusted as the armature entry speed changes because the same armature is accelerated by different stages. As for the parameters of the driving coil, its inner diameter can usually be directly determined based on the known outer diameter of the armature, and the aspect ratio of the driving coil should gradually transition from short and thick coils to long and thin coils as the number of device stages increases, with the number of turns gradually decreasing.

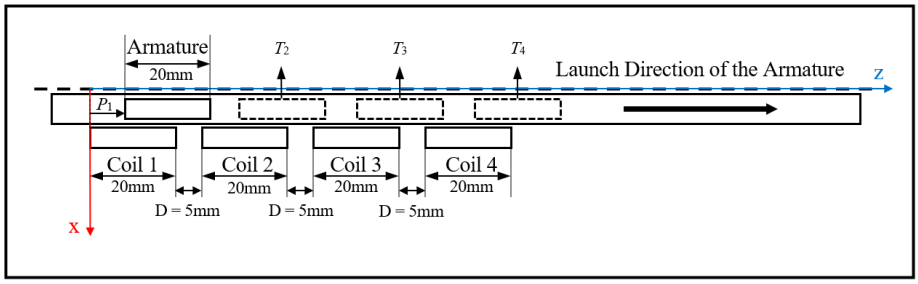

Figure 2. 2D axisymmetric models of the four-stage SICL.

The coil launching devices of the PP and PN configurations studied in this article are shown in Figure 3, and the drive coils are arranged coaxially with the armature. Figure 3a shows the PP configuration launching device with same-direction current applied to the drive coils of the four stages, while Figure 3b shows the PN configuration launching device with alternating reverse-direction current applied to the drive coils of the four stages. In the process of Maxwell simulation, the properties of the drive coils in the PP configuration are set as positive for stages 1 to 4, while in the PN configuration, the properties of the drive coils in stages 1 and 3 are set as positive, and the properties of the drive coils in stages 2 and 4 are set as negative. This is carried out to achieve the simulation analysis of the two configurations of the launching device.

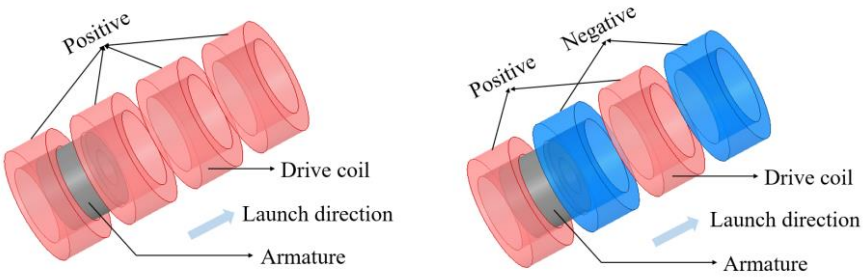

(**a**) (**b**)

Figure 3. Two configurations of coil launching device: (**a**) PP configuration; and (**b**) PN configuration.

In addition, fully charged capacitors are used to discharge the four-stage drive coils, and there is a freewheeling branch in the driving circuit. The external power supply circuit and control circuit of the single-stage drive coil are shown in Figure 4. In this figure, C represents the energy storage capacitor, S represents the pressure-controlled switch, which is controlled by the control circuit to determine its closure status, D represents the diode in the freewheeling branch, and U represents the pulse voltage source. In this article, drive coils of the same specifications are used. In order to match the armature velocity, with the given input energy of 300 J for each stage coil, different power supply parameters are set for the drive coils of stages 1–2 and stages 3–4, as shown in Table 2.

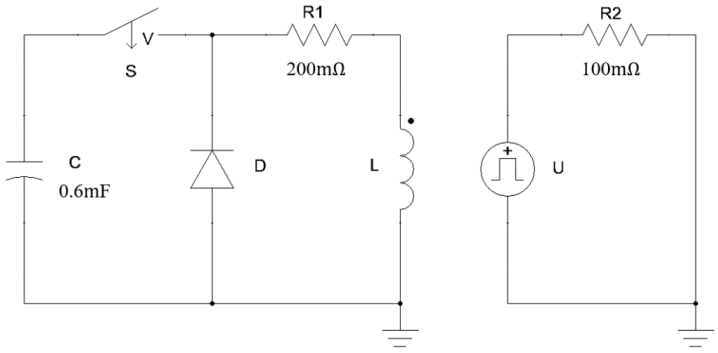

Figure 4. Single-stage drive coil external power supply circuit and control circuit.

Table 2. Power supply parameters of the external circuit.

Pulsed power supply	Stage 1–2	Source capacitance (mF)	0.6
		Charge voltage (kV)	1
	Stage 3–4	Source capacitance (mF)	0.266
		Charge voltage (kV)	1.5

This article adopts a time-triggered circuit triggering method, where the drive coils of each stage are triggered at appropriate times to achieve incremental acceleration of the armature in the launching device. By controlling the external circuit, the required pulse excitation current is provided to the drive coils at the required time. The optimal trigger time for each stage is obtained through simulation experiments to ensure that the device is in the optimal launching state.

2.3. Mathematical Model of SICL

The SICL mainly consists of an accelerating armature, various stages of drive coils, and an external power supply system. During the launching process, there is mutual inductance between each stage of drive coils and between the armature and drive coils. Under the influence of the coil pulse current, the current induced by the armature has non-uniform axial and radial distributions. A common analysis method is to discretize the armature by dividing its cross-section evenly along the axis and unevenly along the radial direction, turning a continuous armature into multiple independent ring armature slices. When the ring cross-section is small enough, it can be approximated that the distribution of induced current on each slice is uniform [12].

Assuming a synchronous induction coil launching device with n drive coils and m armature segments, when the k-th drive coil begins to conduct, the equivalent circuit model is as shown in Figure 5. The current through the drive coils is I_{di} (i = 1, 2, …, k); the resistance of the drive coil loop is R_i (i = 1, 2, …, k); the inductance of the drive coil loop is L_i (i = 1, 2, …, k); the resistance of the loop coil is R_{di} (i = 1, 2, …, k); the inductance of the loop coil is L_{di} (i = 1, 2, …, k); the mutual inductance between the drive coils is M_{ij} (i,j = 1, 2, …, k); the mutual inductance between the drive coils and armature segments is M_{dij} (i = 1, 2, …, k, j = 1, 2, …, m); the mutual inductance between armature segments is M_{pij} (i,j = 1, 2, …, m); the resistance of the armature segment loop is R_{pi} (i = 1, 2, …, m); the self-inductance of the armature loop is L_{pi} (i = 1, 2, …, m); and the current through the armature segment loop is I_{pi} (i = 1, 2, …, m).

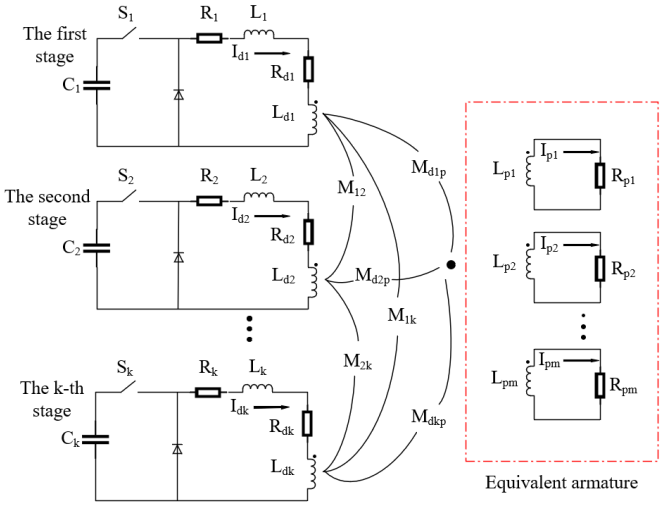

Figure 5. Equivalent circuit model of multi-stage coil launching device.

When considering only the movement direction of the armature as the z-direction and neglecting other energy losses, the force acting on the armature at time t is:

$$F(t) = \sum_{i=1}^{k} \sum_{j=1}^{m} \frac{\mathrm{d}M_{dij}(t)}{\mathrm{d}z} I_{di}(t) I_{pj}(t) \tag{7}$$

From Equation (7), it can be seen that the force on the armature is related to the segments of the armature and the current of the driving coil as well as the mutual inductance gradient. The mutual inductance gradient depends on the relative position between the driving coil and the armature segments. When the armature segments pass through the centerline of the driving coil, the mutual inductance gradient between the driving coil and the armature segments is positive; otherwise, it is negative. Therefore, the magnitude and direction of the current in the armature segments directly determine the force on the armature.

Due to the change in flux, induced currents are generated in the armature segments, and the current induced in the armature segment coil is:

$$I_{pj} = \frac{1}{Z} \frac{\mathrm{d}\varphi}{\mathrm{d}t} = \frac{\mu}{Z} \int \frac{\mathrm{d}H}{\mathrm{d}t} \mathrm{d}A \tag{8}$$

In the formula, φ represents the magnetic flux passing through the armature segment; Z is the impedance of the armature segment; and A is the effective area surrounded by the armature segment.

The change in the axial component of the magnetic field results in the current in the armature segment, thus the rate of change of the axial component of the magnetic field is calculated as:

$$\frac{\mathrm{d}H_z}{\mathrm{d}t} = \frac{\partial H_z}{\partial I_{di}} \cdot \frac{\mathrm{d}I_{di}}{\mathrm{d}t} + \frac{\partial H_z}{\partial z} \cdot \frac{\mathrm{d}z}{\mathrm{d}t} \tag{9}$$

Therefore, the armature winding current can be represented as:

$$I_{pj} = \frac{\mu}{Z} \int \left(\frac{\partial H_z}{\partial I_{di}} \cdot \frac{\mathrm{d}I_{di}}{\mathrm{d}t} + \frac{\partial H_z}{\partial z} \cdot \frac{\mathrm{d}z}{\mathrm{d}t} \right) \mathrm{d}A \tag{10}$$

From Equation (10), it can be seen that the armature segment current consists of two parts: one is caused by the change in drive coil current, defined as induced current; and the other is caused by the movement of the armature segment, defined as motion-induced current. The current in the armature segment is the sum of induced current and motion-induced current.

During the motion of the armature, the magnetic field changes unevenly along the axial direction, leading to inconsistent current distribution among the armature segments. At the same moment, different current densities with opposite directions may exist on the cross-section of the armature. This results in significant force differences among the armature segments, adding complexity to the analysis of the armature's motion mechanism and patterns.

3. Simulation Results and Analysis

In the four-stage induction coil launching device, the armature is initially accelerated from rest by the first-stage drive coil. By changing the triggering position of the armature in the first-stage coil (with the aligned position between the armature and the left side of the drive coil as the zero triggering position), the optimal exit velocity of the first stage is obtained, thus determining the optimal triggering position P_1 of the armature in the first stage. The timing of the acceleration of the armature by the subsequent three stages is determined by changing the excitation triggering time of each stage coil T_i (where i = 2, 3, and 4), and then comparing and analyzing the armature velocity curves obtained by optimizing the triggering timing for both the PP and PN configurations of the launching device.

Meanwhile, in order to explore the influence of the inter-stage distance D on the armature velocity of the two configuration launching devices, simulation experiments are carried out for the launching devices with D = 5 mm and D = 15 mm.

3.1. Obtaining the Optimal Exit Velocity

Figure 6 displays the variation curves of the armature velocity with P and T for the PP and PN configuration launching devices with an inter-stage distance of D = 5 mm. Figure 7 displays the variation curves of the armature velocity with P and T for the PP and PN configuration launching devices with an inter-stage distance of D = 15 mm.

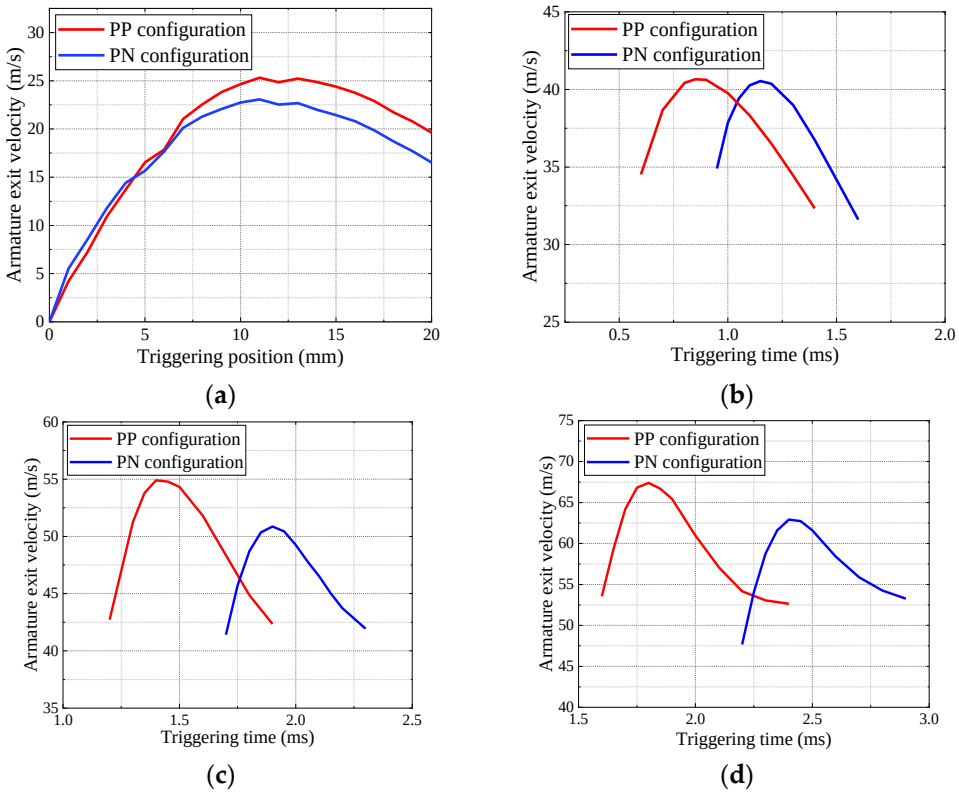

Figure 6. The variation curves of the armature velocity with an inter-stage distance of D = 5 mm: (**a**) in the first-stage coil; (**b**) in the second-stage coil; (**c**) in the third-stage coil; and (**d**) in the fourth-stage coil.

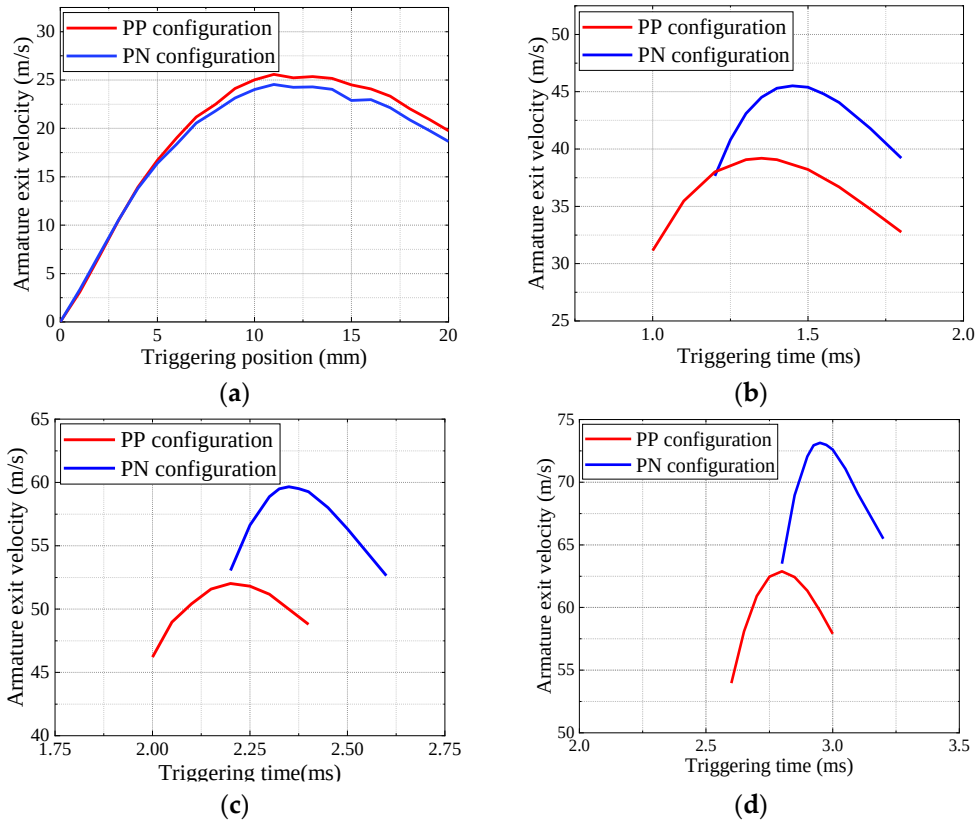

Figure 7. The variation curves of the armature velocity with an inter-stage distance of D = 15 mm: (**a**) in the first-stage coil; (**b**) in the second-stage coil; (**c**) in the third-stage coil; and (**d**) in the fourth-stage coil.

Firstly, in the simulation of PP and PN configurations, the stationary armature is triggered from different initial positions, giving a certain increment to the first-stage triggering position P_1 of the armature. The optimal P_1 is obtained through successive experiments. In this process, although no pulse excitation current is applied to the subsequent three driving coils, the acceleration of the armature is still influenced by the induced currents in the subsequent three driving coils, which are induced by the excitation current in the first-stage coil. Figures 6a and 7a display the variation of armature velocity with the first-stage coil P_1 for the PP and PN configurations of the launching device, respectively. It can be observed that these two configurations have the same optimal P_1, and the armature velocity through the first-stage coil is slightly higher for the PP configuration compared to the PN configuration, which is due to the influence of the induced currents in the subsequent coils.

Based on the analysis above, the optimal triggering position P_1 for the armature to reach the highest velocity in the first-stage drive coil of both configurations is determined. Then, the armature is accelerated with a certain initial velocity into the second-stage drive coil. In this article, the optimal triggering time T_2 for the second-stage coil is obtained through successive experiments by incrementally varying the triggering time. Figures 6b and 7b display the variation of armature velocity with the triggering time T_2 of the second-stage coil for the PP and PN configurations of the launching device, respectively.

After obtaining the optimal triggering position P_1 for the first-stage coil and the optimal triggering time T_2 for the second-stage coil, the optimal triggering time T_3 for the third-stage coil is obtained by incrementally changing the triggering time and conducting successive experiments. Figures 6c and 7c display the variation of armature velocity with the triggering time T_3 of the third-stage coil for the PP and PN configurations of the launching device, respectively.

Finally, the armature is accelerated using the optimal triggering positions and times for the first three stages. The optimal triggering time T_4 for the fourth-stage coil is obtained by incrementally changing the triggering time and conducting successive experiments. Figures 6d and 7d display the variation of armature velocity with the triggering time T_4 of the fourth-stage coil for the PP and PN configurations of the launching device, respectively.

This article uses the optimal trigger timing obtained from simulations as the trigger sequence for the device. The trigger sequence is listed in Table 3. As can be seen from Figure 6, the optimal armature velocities after the second, third, and fourth stages of the PP configuration are higher than those of the PN configuration, and the triggering times of the PN configuration are delayed at each stage. However, in Figure 7, it is the PN configuration that achieves higher optimal armature velocities after the second, third, and fourth stages, while the triggering times of the PN configuration are also delayed at each stage. Therefore, different coil launching devices with different inter-stage distances of D = 5 mm and D = 15 mm have different acceleration effects on the armature. The reasons for this phenomenon will be further investigated in this article.

Table 3. The trigger sequence of the device.

Configuration	D (mm)	P_1 (mm)	T_2 (ms)	T_3 (ms)	T_4 (ms)
PP	5	11	0.85	1.40	1.80
	15	11	1.35	2.20	2.80
PN	5	11	1.15	1.90	2.40
	15	11	1.45	2.35	2.95

3.2. Analysis of the Differences in Acceleration Effects between the Two Configurations

In Figures 8 and 9, the velocity variation curves of the armature from the first to the fourth stage in the PP and PN configurations of the launching device are shown in Figures 8a and 9a, respectively. The axial force variation curves are shown in Figures 8b and 9b. The current curves of each drive coil in the PP configuration are shown in Figures 8c and 9c, and the current curves in the PN configuration are shown in Figures 8d and 9d. The armature triggering is performed according to the optimal P_1, T_2, T_3, and T_4 obtained from the previous simulation experiments for both the PP and PN configurations. It is observed that in the coil launching device with an inter-stage distance of D = 15 mm, the optimized PN configuration achieves higher velocity than the PP configuration, which is consistent with the conclusions obtained by scholars in recent years (i.e., reverse current in the coil helps to improve the exit velocity of the armature). However, in the coil launching device with an inter-stage distance of D = 5 mm, the velocity of the PN configuration does not surpass that of the PP configuration. The following analysis is conducted to explain these phenomena.

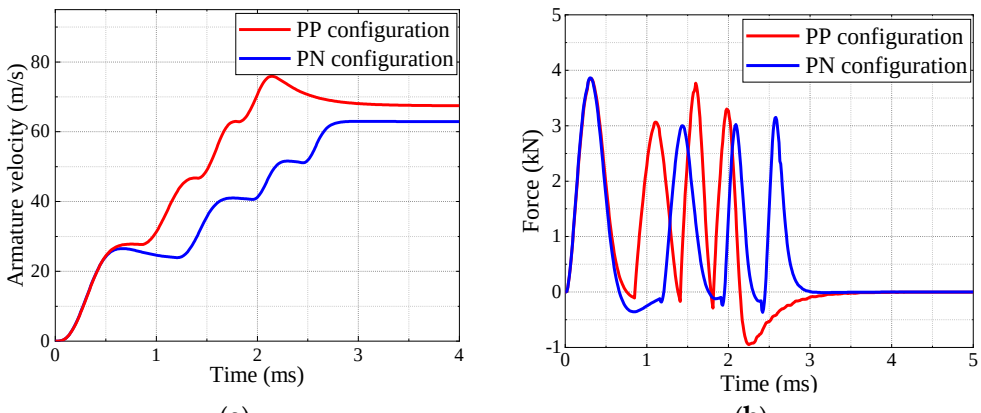

(**a**) (**b**)

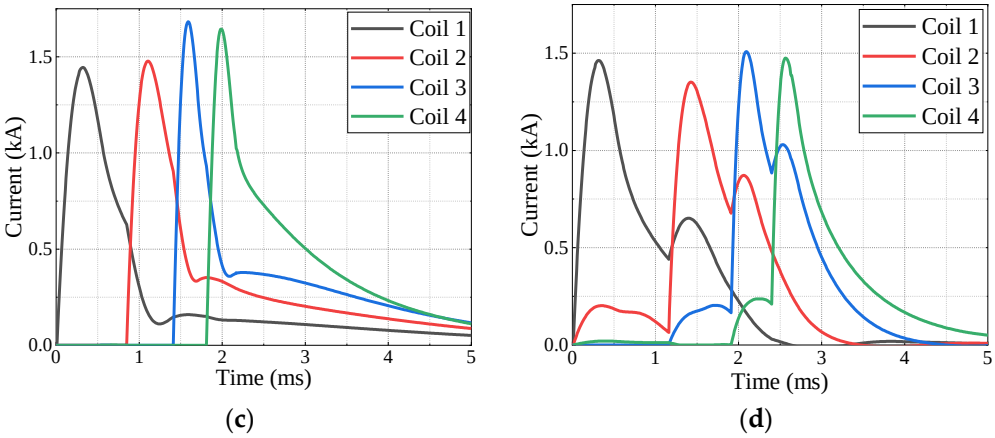

Figure 8. The launching situation of the device with an inter-stage distance of $D = 5$ mm: (**a**) velocity variation curve; (**b**) force variation curve; (**c**) current curve of PP configuration; and (**d**) current curve of PN configuration.

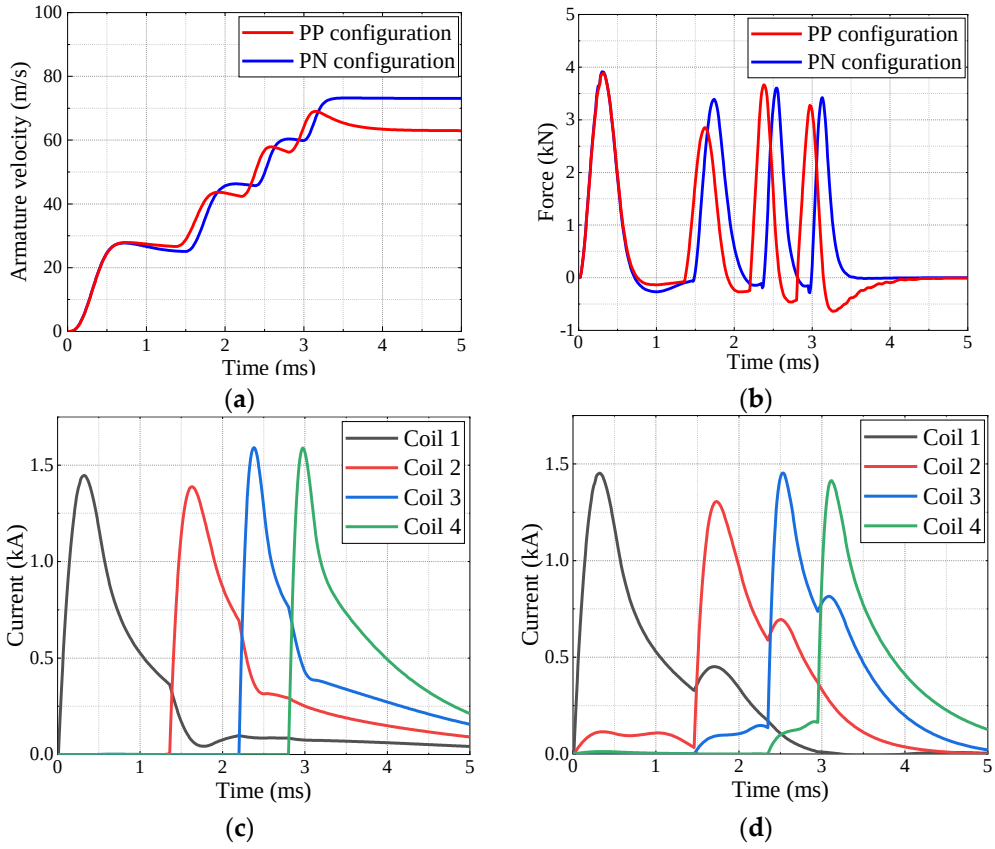

Figure 9. The launching situation of the device with an inter-stage distance of $D = 15$ mm: (**a**) velocity variation curve; (**b**) force variation curve; (**c**) current curve of PP configuration; and (**d**) current curve of PN configuration.

From Figures 8a and 9a, it can be observed that the armature in the PP configuration of the launching device does not exhibit the armature capture effect after being accelerated by the first three drive coils, but experiences significant deceleration due to a large braking force after leaving the fourth-stage coil. Conversely, the armature in the PN configuration experiences a certain armature capture effect after being accelerated by the first three drive coils, resulting in a decrease in velocity after each stage. However, when it leaves the final-stage coil, there is almost no decrease in velocity. This leads to the PP configuration having a higher exit velocity than the PN configuration for D = 5 mm.

The electromagnetic forces acting on the armature in Figures 8b and 9b during the launch process can be correlated with the results in Figures 8a and 9a. For example, the armature in the PN configuration experiences a period of smaller braking forces after being driven by the first three coils, while the armature in the PP configuration only experiences significant deceleration after leaving the final-stage coil. Additionally, the electromagnetic forces acting on each drive coil in the PP configuration occur earlier than in the PN configuration, matching the armature velocity curves.

Comparing (c) and (d) in Figures 8 and 9, it can be found that in the PN configuration of the coil launching device, there is a relatively small induced current generated in the subsequent drive coil after the triggering of the drive coil, and when the subsequent drive coil is energized, the current in that coil is enhanced. In the PP configuration, however, a different phenomenon occurs. The energization of the drive coils does not affect the generation of induced currents in the subsequent drive coils but instead rapidly decreases the induced current in the previous drive coil. This is because there are diodes in the drive coils that restrict the flow of current. In the PN configuration of the coil launching device, the current directions in adjacent drive coils are opposite, resulting in the diodes conducting due to the induced electromotive force. In the PP configuration, the current directions in adjacent drive coils are the same, resulting in the induced electromotive force hindering the conduction of the diodes, thus no induced current is generated.

The maximum axial force density exerted on the armature by the second- to fourth-stage coils in both the PP and PN configurations, for inter-stage distances of $D = 5$ mm and $D = 15$ mm, are shown in Figures 10 and 11 respectively, with units of $\mathrm{kN/m^3}$.

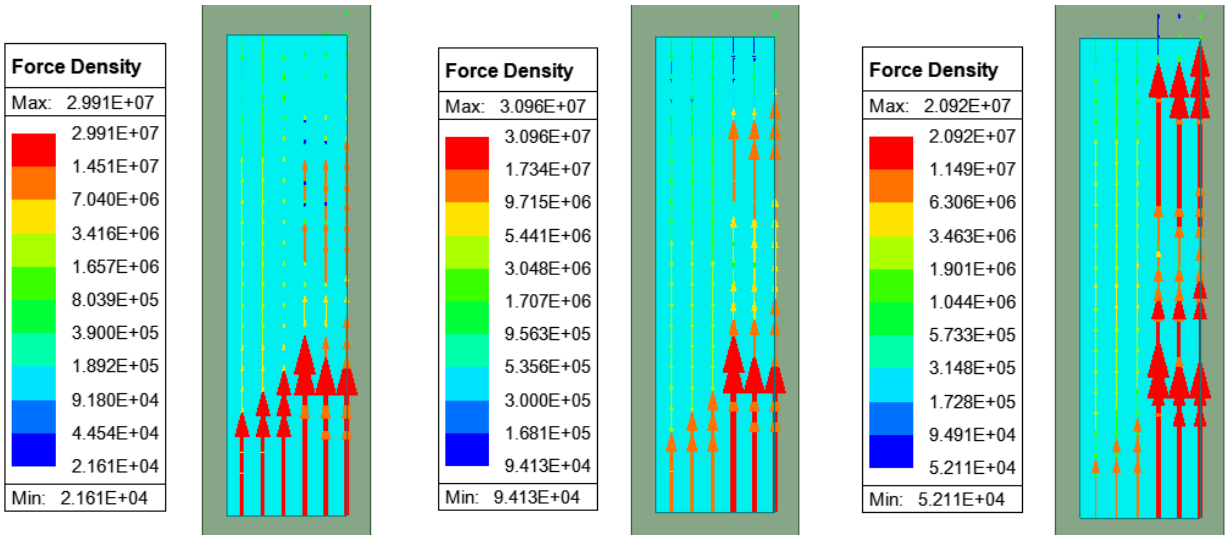

(**a**) (**b**) (**c**)

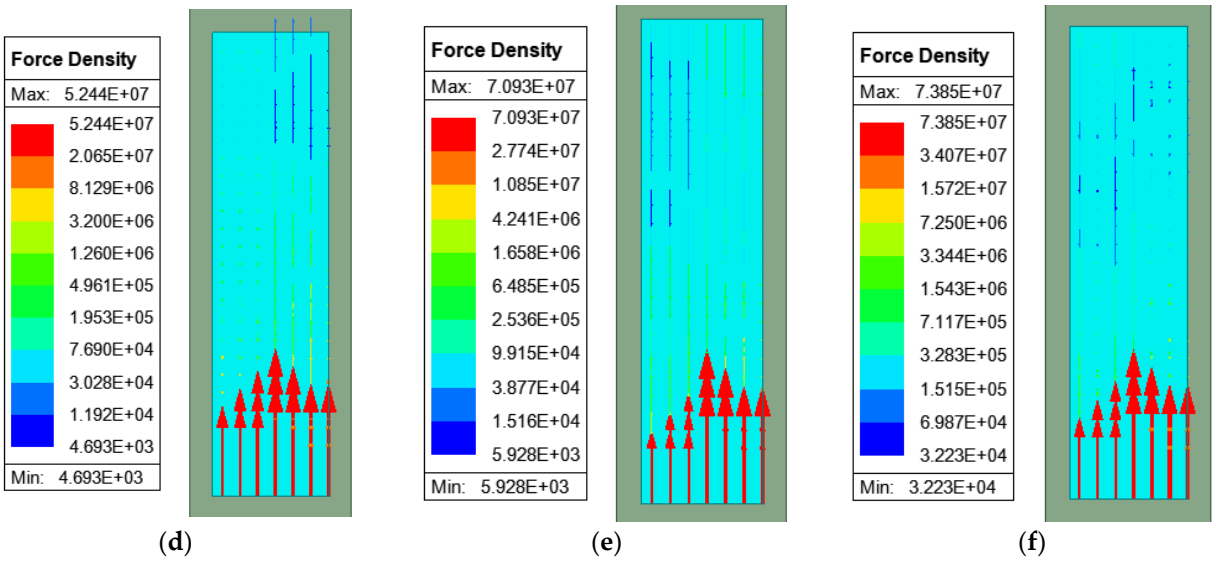

Figure 10. Axial force density (with units of kN/m^3) of the armature with an inter-stage distance of D = 5 mm: (**a**) PP at 1.11 ms; (**b**) PP at 1.60 ms; (**c**) PP at 1.98 ms; (**d**) PN at 1.44 ms; (**e**) PN at 2.09 ms; and (**f**) PN at 2.58 ms.

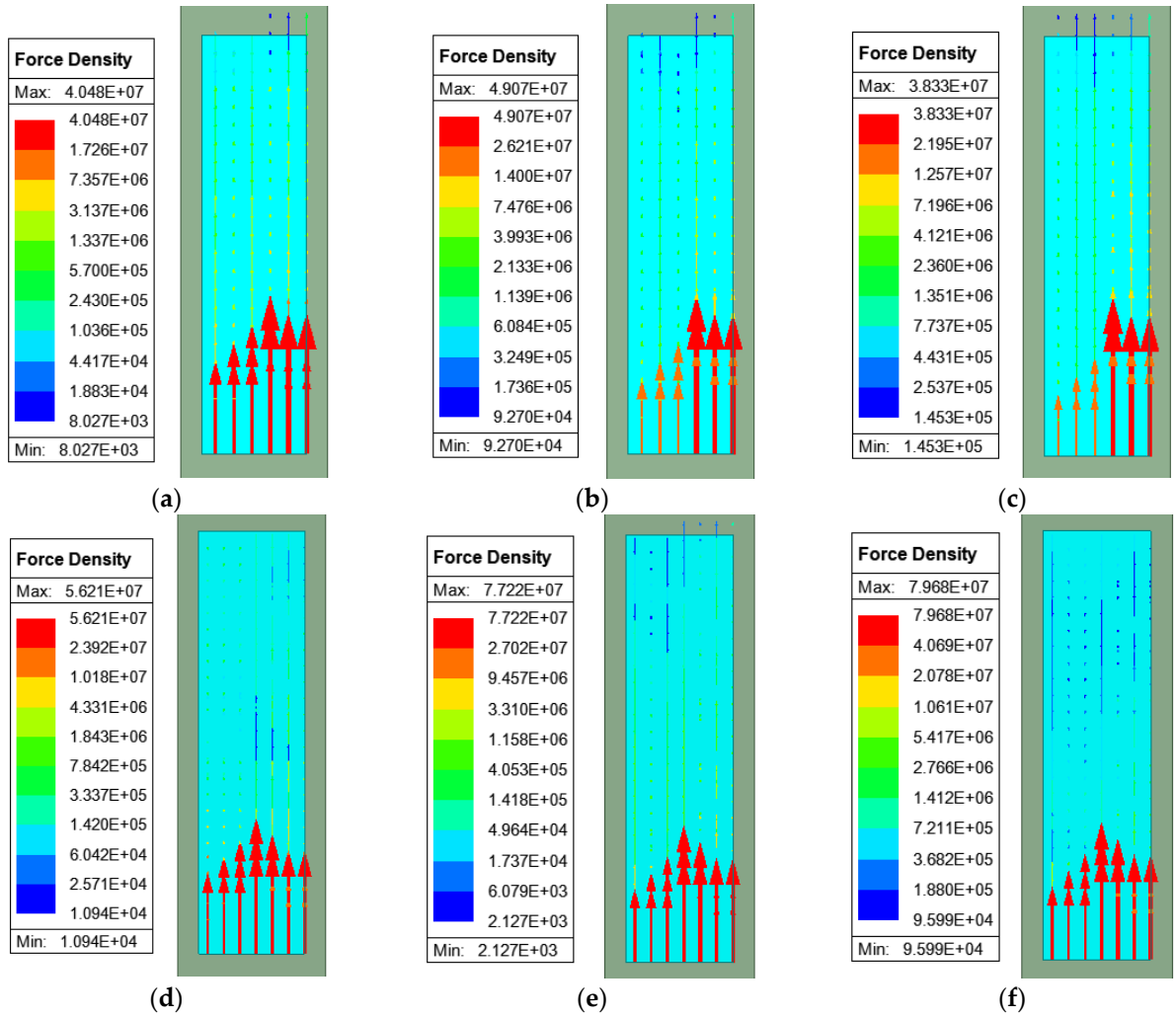

Figure 11. Axial force density (with units of kN/m^3) of the armature with an inter-stage distance of D = 15 mm: (**a**) PP at 1.62 ms; (**b**) PP at 2.38 ms; (**c**) PP at 2.97 ms; (**d**) PN at 1.74 ms; (**e**) PN at 2.54 ms; and (**f**) PN at 3.13 ms.

Figures 10 and 11 show the axial force density cloud maps on the armature at different time points. Despite the different methods of energizing the driving coils, the armature experiences electromagnetic force accelerating it forward, primarily concentrated at the bottom of the armature. It can be observed that the armature has a greater axial force density in the PP configuration at D = 15 mm compared to the device at D = 5 mm, whereas the axial force density on the armature in the PN configuration shows little difference across different time points, consistent with the simulation results of the force curves obtained.

3.3. Mechanism Analysis of the Interaction between the Previous and Next Drive Coils and the Armature

The presence of induced currents in the drive coils can have an impact on the acceleration effect of the armature. Therefore, an analysis and study on this effect is conducted. The electromagnetic force exerted on the armature in the drive coils can be expressed as:

$$F = \frac{\mathrm{d}M}{\mathrm{d}x} i_d i_p \tag{11}$$

In the equations, "i_d" represents the current in the drive coil, "i_p" represents the induced current in the armature, and "dM/dx" represents the gradient of mutual inductance with respect to the position of the armature.

The electromagnetic force exerted on the armature by the preceding-stage drive coil can be expressed as:

$$F_{n-1} = \frac{\mathrm{d}M}{\mathrm{d}x} i_{d(n-1)} i_p \tag{12}$$

The electromagnetic force exerted on the armature by the subsequent-stage drive coil can be expressed as:

$$F_{n+1} = \frac{\mathrm{d}M}{\mathrm{d}x} i_{d(n+1)} i_p \tag{13}$$

As can be seen from Equations (11), (12), and (13), the electromagnetic force exerted on the armature is proportional to the gradient of mutual inductance between the armature and drive coil, as well as the currents in both the armature and drive coil. When the armature is in front of the center of the drive coil, the mutual inductance gradient is positive. If the currents in the armature and drive coil flow in the same direction, the electromagnetic force is a driving force; if they flow in opposite directions, the electromagnetic force is a braking force. When the armature passes through the center of the drive coil, the mutual inductance gradient becomes negative. If the currents in the armature and drive coil flow in the same direction, the electromagnetic force is a braking force; if they flow in opposite directions, the electromagnetic force is a driving force. Figure 12 displays the current density distribution at different times. In Figure 12a, at 0.4 ms, the induced current in the armature is in the opposite direction to the current in the first-stage coil, resulting in a driving force on the armature. In Figure 12b, at 0.8 ms, the induced current in the armature is in the same direction as the current in the first-stage coil, resulting in a braking force on the armature.

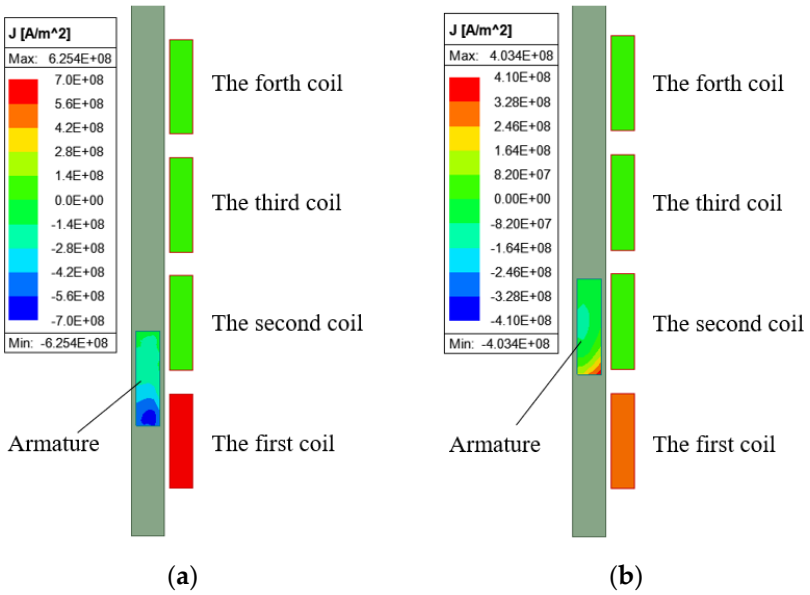

Figure 12. Current density contour maps of the launching device at different time points: (**a**) at 0.4 ms; and (**b**) at 0.8 ms.

This article analyzes the entire process of the armature being accelerated by the corresponding drive coil, dividing it into an acceleration section and a deceleration section influenced by the armature capture effect, as shown in Figure 13. In the PN configuration coil launcher, the induced current in the previous and next drive coils is opposite to the current flowing in the nth-stage coil. As can be seen from Equations (1), (2), and (3), during the acceleration stage of the nth-stage coil, the (n − 1)th-stage coil provides acceleration force to the armature, while the (n + 1)th-stage coil provides braking force to the armature. During the deceleration stage of the nth-stage coil, the (n − 1)th-stage coil provides braking force to the armature, while the (n + 1)th-stage coil provides acceleration force to the armature. In the PP configuration coil launcher, the induced current in the (n − 1)th-stage coil is in the same direction as the current flowing in the nth-stage coil, and there is no induced current in the subsequent stages when the nth-stage coil is energized. During the acceleration stage of the nth-stage coil, the (n − 1)th-stage coil provides braking force to the armature, while during the deceleration stage of the nth-stage coil, the (n − 1)th-stage coil provides acceleration force to the armature. In both configurations of the drive coil, the forces acting on the armature by the previous and next drive coils during the two stages of launching are shown in Table 4.

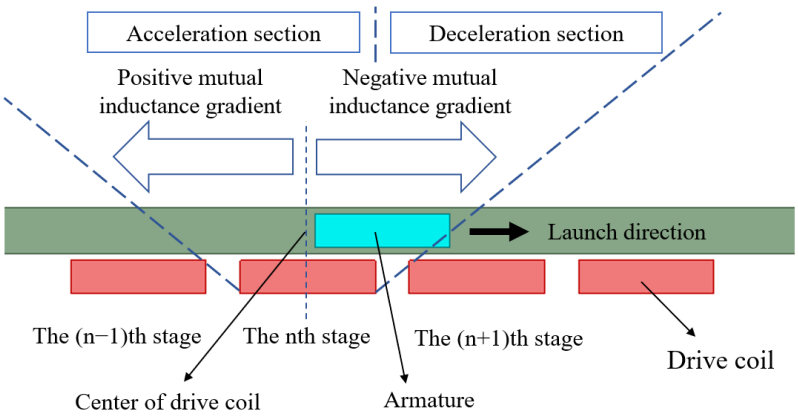

Figure 13. Mechanism analysis schematic diagram.

Table 4. In both configurations, the armature experiences the forces exerted by the previous and next drive coils during the two stages of the launch process.

Configuration	The nth-Stage Coil	The (n − 1)th-Stage Coil	The (n + 1)th-Stage Coil
PN	Acceleration section	Braking force	Acceleration force (ignored)
	Deceleration section	Acceleration force (ignored)	Braking force
PP	Acceleration section	Acceleration force	—
	Deceleration section	Braking force (ignored)	—

The magnitude of the electromagnetic force on the armature by the drive coil is dependent on the distance to this coil [17]. In both configurations of the launching device, the influence of the (n + 1)th-stage coil on the armature during the acceleration stage and the influence of the (n − 1)th-stage coil on the armature during the deceleration stage are not considered in order to simplify the analysis and focus on the more significant factors. As a result, in the PN configuration coil launcher, the previous and next drive coils mainly provide a deceleration effect on the armature, while in the PP configuration coil launcher, the previous and next drive coils mainly provide an acceleration effect on the armature.

Therefore, in the launching device with a distance D = 5 mm between each drive coil, as shown in Figure 8a, the PP configuration armature exit velocity is ultimately better than the PN configuration. However, in the launching device with a distance D = 15 mm, the increased distance between the previous and next drive coils and the armature weakens the influence of the drive coils on the armature. This weakens the deceleration effect of the PN configuration and the acceleration effect of the PP configuration, resulting in an enhanced velocity for the PN configuration armature and a relatively reduced velocity for the PP configuration armature. As shown in Figure 9a, the simulation results are consistent with the theoretical analysis mentioned above.

3.4. The Influence of Inter-Stage Distance on the Selection of Current Direction

Based on the previous analysis, it can be preliminarily concluded that different inter-stage distances will affect the coupling relationship between the drive coils and the armature, thereby affecting the electromagnetic force exerted on the armature during the launching process. Inter-stage coupling causes the electromotive force on the drive coil to alternate from positive to negative. When the induced electromotive force and the capacitor voltage are connected in reverse series, the total voltage of the drive coil discharge circuit decreases, which is not conducive to the acceleration of the armature. When connected in the forward series, due to the presence of the freewheel diode, a circuit current will be formed, and some energy will be dissipated as heat on the discharge circuit resistance of the drive coil, leading to a decrease in system transmission efficiency.

Therefore, the smaller the inter-stage distance of the drive coils, the tighter the coupling with the armature, and the more significant the influence of the induced current on the armature. In this case, the armature velocity of the PP configuration is better than that of the PN configuration. As the inter-stage distance of the drive coils increases, the armature velocity of the PP configuration gradually decreases, while the armature velocity of the PN configuration gradually increases, eventually surpassing the armature velocity of the PP configuration.

The simulation results are consistent with the theoretical analysis. By giving a certain linear increment to the inter-stage distance of the drive coils, simulations are conducted on the launching devices with different inter-stage distances. The selection of specific inter-stage distances in our study is based on a combination of practical considerations and the need to explore a range of distances that are commonly encountered in

electromagnetic launch systems. The chosen distances were intended to provide a comprehensive understanding of how variations in inter-stage distance impact system performance.

The triggering time of the excitation current for each drive coil is optimized using the method mentioned earlier, and the optimal exit velocity of each device is obtained. Table 5 lists the simulation data of the optimal armature exit velocity obtained after acceleration by the drive coils of PP and PN configurations at different inter-stage distances, where N represents the number of acceleration stages.

Table 5. Simulation results of the optimal exit velocity for two different configurations at varying stage distances and acceleration stages.

Inter-Stage Distance	2.5 mm (m/s)	5 mm (m/s)	7.5 mm (m/s)	10 mm (m/s)	12.5 mm (m/s)	15 mm (m/s)	17.5 mm (m/s)	20 mm (m/s)	22.5 mm (m/s)
PP: N = 2	41.76	40.66	39.78	39.57	39.05	39.20	39.22	39.27	39.48
PN: N = 2	38.53	40.53	42.23	43.71	44.61	45.52	46.13	46.57	46.99
PP: N = 3	57.68	54.90	53.66	52.95	52.06	52.02	51.68	51.98	52.08
PN: N = 3	47.48	50.86	53.34	55.84	57.94	59.66	60.82	61.64	63.05
PP: N = 4	70.78	67.39	66.43	64.66	63.65	62.88	62.62	62.89	62.79
PN: N = 4	59.28	62.92	66.21	68.67	70.66	73.14	74.19	74.45	76.94

Analyzing the data in Table 5 reveals that in the coil launch device with a PP configuration, the optimal exit velocity gradually decreases as the distance between driving coil stages increases. In contrast, in the coil launch device with a PN configuration, the optimal exit velocity increases as the distance between driving coil stages increases. Furthermore, among the existing data on driving coil stage distances, the optimal exit velocity of the armature for PP configuration is superior to PN configuration within the 2.5 mm–7.5 mm stage distances, while for PN configuration, the 10 mm–22.5 mm range is superior to PP configuration. Figure 14 is obtained through curve fitting of the existing data. Figure 14 displays the optimal exit velocity curves for the two configurations with different adjusted inter-stage distances.

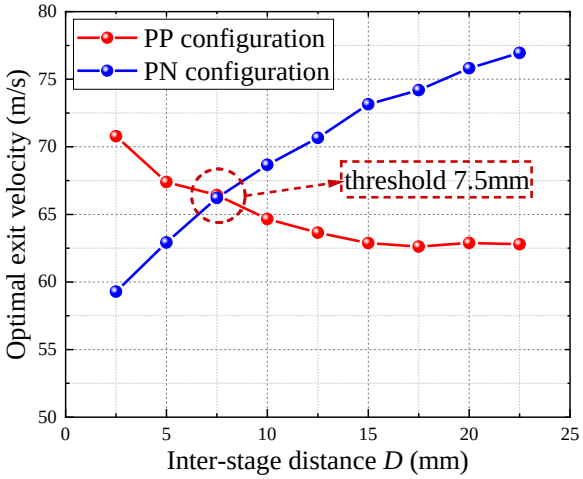

Figure 14. The optimal exit velocity of the armature at different inter-stage distances.

It can be observed from Figure 14 that as the inter-stage distance of the drive coils in the SICL increases, the optimal exit velocity of the PP configuration device gradually decreases and tends to stabilize, while the optimal exit velocity of the PN configuration device gradually increases and tends to stabilize. The intersection point of the two curves represents the threshold value of the inter-stage distance, which is 7.5 mm in this case, accounting for 37.5% of the length of the drive coils. When the inter-stage distance is

smaller than this threshold value, the coil launching device using the PP configuration will achieve a better armature exit velocity. Conversely, when the inter-stage distance is larger than this threshold value, the coil launching device using the PN configuration will achieve a better armature exit velocity.

3.5. Results and Verification

The research conclusion can be summarized by the following equations.

Where L_d represents the length of the driving coil, D represents the distance between driving coil stages, and T represents the threshold of the distance between driving coil stages, which is obtained by the intersection of the two curves in Figure 14.

As shown in Equation (14), in this study, K is defined as the ratio of the threshold T to the length L_d of the driving coil.

$$K = \frac{D}{L_d} \times 100\% \tag{14}$$

When $D = T$, there is a theoretical threshold T for the distance between the driving coil stages. At this point, when the launch device emits the armature by applying power in either the PP or PN methods, although there are differences in the acceleration principles, the same acceleration effect will be achieved. Let K at this time be denoted as K_T and K_T can be calculated as follows:

$$K_T = \frac{T}{L_d} \times 100\% = \frac{7.5\text{ mm}}{20\text{ mm}} \times 100\% = 37.5\% \tag{15}$$

When $K < K_T (D < T)$, the driving coils of the launch device are powered by the PP method. The acceleration effect on the armature will gradually decrease with an increase in inter-stage distance. If powered by the PN method, the acceleration effect on the armature will also gradually decrease with an increase in inter-stage distance. However, the PP method is always superior to the PN method. Therefore, in this case, it is recommended to use the PP method for the launch device.

When $K > K_T (D > T)$, the driving coils of the launch device are powered by the PP method. The acceleration effect on the armature will still gradually decrease with an increase in inter-stage distance. If powered by the PN method, the acceleration effect on the armature will still gradually decrease with an increase in inter-stage distance. However, the PN method is always superior to the PP method. Therefore, in this case, it is recommended to use the PN method for the launch device.

From Equations (14) and (15), it is evident that the optimal power-on method of the launch device is determined by the distance D between different stages based on the parameters T and K_T of the device. The T values in each launch device vary due to the device's different size specifications, while the ratio K is not influenced by the device size. In this study, it is approximated that $K_T = 37.5\%$.

In order to validate and confirm the research findings, ensuring the accuracy and reliability of the study, the analysis results of this research will be applied to the research device model in the existing literature, verifying the consistency with the results of this study under different models of coil launch devices.

In reference [12], where $L_d = 16.3\text{ mm}$ and $D = 10\text{ mm}$, the value of K can be calculated using the following equation:

$$K = \frac{D}{L_d} \times 100\% = \frac{10\text{ mm}}{16.3\text{ mm}} \times 100\% = 61.3\% > K_T \tag{16}$$

The research findings that "The launch velocity in the PN launcher is more than in the PP launcher" are consistent with the optimal power-on method selection in this study.

In reference [13], the launch device adopts the PN power-on method. Simulation is conducted with D ranging from 5 mm to 40 mm. The research shows that as the value of

D increases, the efficiency of the device's energy conversion gradually improves, which is consistent with the conclusion of this study.

In reference [18], where $L_d = 100$ mm and $D = 20$ mm, the value of *K* can be calculated using the following equation:

$$K = \frac{D}{L_d} \times 100\% = \frac{20 \text{ mm}}{100 \text{ mm}} \times 100\% = 20\% < K_T \quad (17)$$

The research finding that "In the design process of a multi-stage synchronous induction coil launcher, adjacent driving coils should be arranged with the same polarity" is consistent with the optimal power-on method selection in this study.

The results obtained in this study are applied to the literature related to the determination of the driving coil energization method. The comparison of the experimental results obtained from different device models with the results of this study all confirm the relationship between the driving coil inter-stage distance and the selection of the energization method. This validates the accuracy and effectiveness of the results of this study.

4. Conclusions

This article discusses the differences in armature acceleration effects based on different inter-stage distances and energization methods. It is pointed out that the distance between stages is the key factor affecting the selection of coil energization direction. To verify this, the article performs field-circuit coupling simulations on a four-stage synchronous induction coil launching device model by ANSYS Maxwell software. The results are as follows:

1. The armature exit velocity of the PP energization method is superior to that of the PN energization method in the device with an inter-stage distance of 5 mm. However, in the device with an inter-stage distance of 15 mm, the armature exit velocity of the PN energization method is superior to that of the PP energization method.
2. In the coil launch device with the PN energization method, the previous and next drive coils mainly provide a deceleration effect on the armature. Conversely, in the coil launch device with the PP energization method, the previous and next drive coils mainly provide an acceleration effect on the armature.
3. Different inter-stage distances affect the coupling relationship between each drive coil and the armature. Increasing the inter-stage distance weakens the effect of the induced current in the coil on the armature launch process.
4. There is a threshold value of 7.5 mm for the inter-stage distance of the drive coils, which accounts for 37.5% of the length of the drive coils. If the inter-stage distance does not exceed this threshold value, selecting the PP energization method for the launch device will result in a better armature exit velocity. However, if the inter-stage distance exceeds this threshold value, selecting the PN energization method for the launch device will result in a better armature exit velocity.

The simulation results of this model are consistent with the theoretical analysis and align with the validation of consistency with other existing studies. That is, the different acceleration modes generated by the two coil energization methods result in a threshold distance between each driving coil, which is a key factor in determining the energization direction of the launcher coil. This conclusion provides a basis for the selection of coil energization methods and valuable references for determining the energization direction of multi-stage SICL coils.

Author Contributions: Conceptualization, Y.G.; methodology, Y.G.; software, Y.G.; validation, Y.G.; formal analysis, X.W.; investigation, Y.G.; resources, X.W.; data curation, Y.G.; writing—original draft preparation, Y.G.; writing—review and editing, Y.G., X.W., and J.K.; visualization, Y.G.; supervision, X.W.; project administration, X.W. and J.K.; funding acquisition, X.W. All authors have read and agreed to the published version of the manuscript.

Funding: This research was funded in part by the Natural Science Basic Research Program of Shaanxi Province Program under Grant 2024JC-YBMS-346, in part by the Natural Science Pre-study Foundation of Shaanxi University of Science and Technology under Grant 2020BJ-53, in part by the Open Fund for Nation-al Engineering Laboratory of Energy-Saving Motor and Control Technology, Anhui University under Project KFKT202205.

Institutional Review Board Statement: Not applicable.

Informed Consent Statement: Not applicable.

Data Availability Statement: Data is contained within the article.

Conflicts of Interest: The authors declare no conflicts of interest.

References

1. Ma, W.; Xiao, F.; Nie, S. Application and development of power electronic technology in electromagnetic launch system. *Trans. China Electrotech. Soc.* **2016**, *31*, 1–10. (In Chinese).
2. Ma, W.; Lu, J.; Liu, Y. Research progress of electromagnetic launch technology. *IEEE Trans. Plasma Sci.* **2019**, *47*, 2197–2205.
3. Zhang, X.; Lu, J.; Li, X.; Guo, Y.; Wu, W. Optimization design of electromagnetic induction coil firing system. *Trans. China Electrotech. Soc.* **2021**, *36*, 4658–4665. (In Chinese).
4. Lu, F. Investigation of synchronous induction coilgun with stepped coil launcher and stepped armature. *IEEE Trans. Plasma Sci.* **2020**, *48*, 1190–1194.
5. Guan, S.; Guan, X.; Guo, D.; Wang, S. Shielding and optimization of high magnetic field in multistage synchronous induction coil launcher armature. *Trans. China Electrotech. Soc.* **2020**, *35*, 333–340. (In Chinese).
6. Ingram, M.W.; Andrews, J.A.; Bresie, D.A. An actively switched pulsed induction accelerator. *IEEE Trans. Magn.* **1991**, *27*, 591–595.
7. Zhang, T.; Guo, W.; Su, Z.; Cao, B.; Sun, X.; Ren, R.; Ge, X.; Li, M. Investigation of magnetic field arrangement on launching performance of multistage synchronous induction coilgun. *IEEE Trans. Plasma Sci.* **2017**, *45*, 1436–1442.
8. Zhang, T.; Guo, W.; Fan, W.; Liu, Y.; Su, Z.; Zhang, H.; Huang, K. Acceleration mechanism and experimental research of multi-Stage synchronous induction coilgun based on magnetic field arrangement. *IEEE Trans. Plasma Sci.* **2019**, *47*, 4753–4759.
9. Zhang, T.; Guo, W.; Su, Z.; Liu, Y.; Fan, W. Efficiency improvement analysis of synchronous induction coil launcher based on magnetic field direction change magnetic field direction change. *Trans. China Electrotech. Soc.* **2021**, *36*, 517–524. (In Chinese).
10. Zhang, T.; Guo, W.; Liu, Y.; Su, Z.; Zhang, H.; Fan, W.-Q.; Huang, K. Study on the characteristics of magnetic-field arrangement of synchronous induction coilgun. *IEEE Trans. Plasma Sci.* **2020**, *48*, 2316–2323.
11. Niu, X.; Feng, J.; Li, W.; Jing, D.; Zhang, Z. Effect of polarity reversal on performance of synchronous induction coil launcher. *IEEE Trans. Plasma Sci.* **2020**, *48*, 1343–1349.
12. Ram, R.; Thomas, M.J. Analysis of the differences in the optimum triggering positions and projectile velocities in multistage induction coilguns for different arrangements of the drive coil current directions. *IEEE Trans. Plasma Sci.* **2020**, *51*, 2069–2078, July 2023.
13. Zheng, F.; Huang, C.; Jiang, R.; Lu, M.; Qian, H. Analysis and optimization method of the influence of power mode on the performance of multistage synchronous induction coil device. *J. Ordnance Equip. Eng.* **2022**, *43*, 165–171. (In Chinese).
14. Zhang, Y.; Xiao, G.; Gong, Y.; Niu, X.; Liu, K. Armature structure research of a synchronous induction coil launcher. *IEEE Trans. Plasma Sci.* **2017**, *45*, 1574–1578.
15. Camp, J.T. Optimizing coilgun geometry to maximize efficiency. *IEEE Trans. Plasma Sci.* **2022**, *50*, 3816–3823.
16. Niu, X.; Liu, K.; Zhang, Y.; Xiao, Z.; Gong, Y. Research on adaptive design of multistage synchro-nous induction coil launcher. *Trans. China Electrotech. Soc.* **2018**, *33*, 3644–3650. (In Chinese).
17. Ram, R.; Thomas, M.J. Effect of mutual magnetic flux linkage between stages of an induction coilgun on its performance. *IEEE Trans. Plasma Sci.* **2022**, *50*, 2285–2292.
18. Zhao, K.; Li, Z.; Zhang, Q.; Xiang, H.; Lei, B.; Lü, Q. Influence of polar arrangement manner of driving coil on accelerative performance of multi-stage synchronous induction coil launcher. *J. Acad. Armored Force Eng.* **2014**, *28*, 61–65. (In Chinese).